

SUPPLEMENTARY MATERIAL

A novel xanthone dimer derivative with antibacterial activity isolated from the bark of *Garcinia mangostana*

Weiyi Wang^{a,b,c,†}, Yanyan Liao^{a,b,d,†}, Xiaomei Huang^{a,b,d}, Chao Tang^{a,b,d} and Peng Cai^{a,b,d*}

^a Key Laboratory of Urban Environment and Health, Institute of Urban Environment, Chinese Academy of Sciences, Xiamen 361021, Fujian, P. R. China; ^b University of Chinese Academy of Sciences, Beijing 100049, P. R. China; ^c State Key Laboratory Breeding Base of Marine Genetic Resources, Fujian Key Laboratory of Marine Genetic Resources, Fujian Collaborative Innovation Centre for Exploitation and Utilization of Marine Biological Resources, Third Institute of Oceanography, State Oceanic Administration, Xiamen 361005, Fujian, P. R. China; ^d Xiamen Key Laboratory of Physical Environment, Xiamen 361021, Fujian, P. R. China

† These authors contributed equally to this work

Abstract: A novel xanthone dimer derivative, garmoxanthone (**1**), together with ten known compounds (**2-11**), were isolated from bark of *Garcinia mangostana*. Their structures were established through spectroscopic methods. Garmoxanthone exhibited strong inhibitory activities against MRSA ATCC 43300 and MRSA CGMCC 1.12409 (with MIC values of both 3.9 µg/mL) and moderate activities against tested strains of *Vibrio* (with MIC values ranging from 15.6 to 31.2 µg/mL). Garmoxanthone is a unique xanthone dimer with linkage of a fused 5/6 ring system and its absolute configuration was elucidated on the basis of experimental and calculated electronic circular dichroism. Garmoxanthone exhibited strong antibacterial activity which partially validated the ethnobotanical use of *G. mangostana* in the treatment of infections.

Keywords: *Garcinia mangostana*; xanthone dimer; garmoxanthone; antibacterial

1. Experimental

1.1. General

1D NMR and 2D NMR spectra were recorded on a Bruker DRX-600 instrument. HRESIMS were carried out on Bruker Daltonics Apex ultra 7.0 T Fourier transform mass spectrometer with an Electrospray ionization source (Apollo II, Bruker Daltonics, Bremen, Germany). For column chromatography (CC), RP-C18 (ODS-A, 50 μ m, YMC, Japan), silica gel (200-300 mesh, 300-400 mesh, Branch of Qingdao Marine Chemical Co. Ltd, China), and Sephadex LH-20 (GE Healthcare Bio-Science AB, USA) were used. The HPLC analysis was performed on a Waters 2695-2998 high performance liquid chromatography (Waters, USA). The UV spectrum was recorded on a UV-1800 spectrophotometer (Shimadzu, Japan). Semi-preparative HPLC was run with a P3000 pump (CXTH, China) and a UV3000 ultraviolet-visible detector (CXTH, China) using a preparative RP-C18 column (5 μ m, 20 \times 250 mm, YMC, Japan). Thin-layer chromatography (TLC) plates (5 \times 10 cm plates) were performed on GF254 (Branch of Qingdao Marine Chemical Co. Ltd, China) plates.

1.2. Plant material

The fresh *G. mangostana* of Thailand was purchased from Xiamen market in August 2014. A voucher specimen (No. 20140815-SZ) has been deposited in Key Laboratory of Urban Environment and Health, Institute of Urban Environment, Chinese Academy of Sciences, China.

1.3. Extraction and isolation

The bark of *G. mangostana* was collected from fresh fruits and milled with a grinder. 2 kg of dried material was extracted with 70% ethanol to obtain crude extract (260 g). The extract was partitioned between PE and H₂O and then between EtOAc and H₂O. Removal of the solvent of the EtOAc extract gave 180 g of residue, which was subject to a silica gel (300-400 mesh) column chromatography, eluting with PE-Acetone (9:1, 8.5:1.5, 7.5:2.5, 7:3, 5:5, 4:6, 3.5:6.5, V:V) to yield seven fractions A-G. Further separation of fraction B (8.5:1.5, 25 g) was applied to silica gel column chromatography (300-400 mesh) using PE-acetone and semi-preparative HPLC (80% MeOH in H₂O,

flow rate 8 ml/min) to give **10** (26 mg) and **11** (12 mg). Fraction C (7.5:2.5, 30 g) was further purified by semi-preparative HPLC (67% MeOH in H₂O, flow rate 8 ml/min) and Sephadex LH-20 (MeOH) to give **1** (20 mg), **2** (19 mg), **5** (8 mg) and **6** (10 mg). Fraction E (5:5, 120 g) was further purified by silica gel (300-400 mesh) column chromatography, eluting with hexane-EtOAc (7:3, V:V) and Sephadex LH-20 (MeOH) to obtain **3** (10.8 mg), **4** (5.6 mg), **7** (17.4 mg) and **8** (8.5 mg). Fraction G (3.5:6.5, 16 g) was further separated by semi-preparative HPLC (70% MeOH in H₂O, flow rate 8 ml/min), Sephadex LH-20 (80% MeOH in H₂O) and preparative TLC to obtain **9** (10 mg).

1.4. Garmoxanthone (1)

C₃₆H₂₈O₁₂, grayish yellow amorphous powder; UV λ_{\max} (MeOH) nm (log ϵ): 331 (4.53); $[\alpha]_D^{20.0}$ 156.2 (c 0.16, MeOH); ¹H NMR and ¹³C NMR data are shown in Table S3; HR-ESI-MS: m/z 675.14747 [M+Na]⁺ (Calcd for 675.14785, C₃₆H₂₈O₁₂Na).

1.5. Antibacterial assays

Antibacterial activity against MRSA (ATCC 43300), MRSA (CGMCC1.12409), *Vibrio rotiferianus* (MCCC E385), *Vibrio vulnificus* (MCCC E1758) and *Vibrio campbellii* (MCCC E333) was tested by the continuous dilution in 96-well plates using resazurin as surrogate indicator. Oxidoreductase of viable bacteria reduced blue resazurin to pink resorufin. Mid-logarithmic-phase tested strain was added at a starting inoculum of 5×10⁵ CFU/ml to the test plate containing the serially diluted compound plus 10% resazurin solution (6.75 mg/ml in sterile water). The plate was covered with foil and incubated for 24 h with shaking at 37°C. After overnight incubation, the plate was evaluated visually for blue-to-pink color change. The MIC was determined to be the lowest concentration that did not induce the color change (Haste et al. 2011, Wang et al. 2017).

1.6. ECD calculation

Conformational analysis was initially performed using Confab (O'Boyle et al. 2011) at MMFF94 force field for all configurations. Room-temperature equilibrium populations were calculated according to Boltzmann distribution law (eq.1). The conformers with

Boltzmann-population of over 1% were chosen for ECD calculations. The energies and populations of all dominative conformers were provided in Table S1.

$$\frac{N_i}{N} = \frac{g_i e^{-\frac{E_i}{k_B T}}}{\sum g_i e^{-\frac{E_i}{k_B T}}} \quad (\text{eq. 1})$$

N_i is the number of conformer i with energy E_i and degeneracy g_i at temperature T , and k_B is Boltzmann constant.

The theoretical calculation was carried out using Gaussian 09. First, the chosen conformer was optimized at PM6 using semi-empirical theory method, and then optimized at B3LYP/6-311G** in MeOH using the CPCM polarizable conductor calculation model (Table S2). The theoretical calculation of ECD was conducted in MeOH using Time-dependent Density functional theory (TD-DFT) at the same theory level. Rotatory strengths for a total of 50 excited states were calculated. The ECD spectrum is simulated in SpecDis(Bruhn et al. 2013) by overlapping Gaussian functions for each transition.

References

- Bruhn T, Schaumlöffel A, Hemberger Y, Bringmann G. 2013. SpecDis: quantifying the comparison of calculated and experimental electronic circular dichroism spectra. *Chirality*. Apr;25:243-249.
- Haste NM, Hughes CC, Tran DN, Fenical W, Jensen PR, Nizet V, Hensler ME. 2011. Pharmacological properties of the marine natural product marinopyrrole A against methicillin-resistant *Staphylococcus aureus*. *Antimicrobial agents and chemotherapy*. Jul;55:3305-3312.
- O'Boyle NM, Vandermeersch T, Flynn CJ, Maguire AR, Hutchison GR. 2011. Confab - Systematic generation of diverse low-energy conformers. *J Cheminform*. Mar 16;3:8.
- Wang W, Chen R, Luo Z, Wang W, Chen J. 2017. Two new benzoate derivatives and one new phenylacetate derivative from a marine-derived fungus *Engyodontium album*. *Natural product research*. Apr;31:758-764.

Table **S1**. Energies of the dominative conformers at MMFF94 force field

Configuration	Conformer	Energy (kcal/mol)	Population (%)
11- <i>R</i> , 12- <i>R</i> , 17- <i>S</i>	1	133. 99	100
11- <i>S</i> , 12- <i>S</i> , 17- <i>R</i>	1	126. 11	100

Table **S2**. Energies of the conformers at B3LYP/6-311G** in methanol.

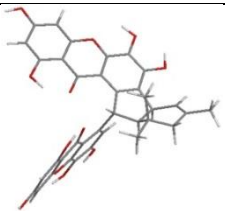
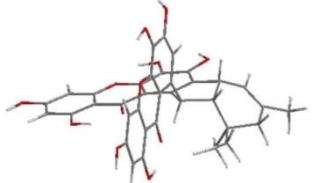
Configuration	Conformation	Structure	E (Hartree)	E (kcal/mol)	Population (%)
11- <i>R</i> , 12- <i>R</i> , 17- <i>S</i>	1		-2292.018376	-1438263.23	100
11- <i>S</i> , 12- <i>S</i> , 17- <i>R</i>	1		-2292.032523	-1438272.11	100

Table S3. ¹H-NMR (600 MHz), ¹³C-NMR (150 MHz) and 2D-NMR data for compound **1** (DMSO-*d*₆).

Position	δ_C , type	δ_H , mult (J_{Hz})	COSY	HMBC	NOESY
1	163.7, C				
2	98.3, CH	6.12, br d (1.76)		C-1, 3, 4, 9a	
3	165.2, C				
4	94.0, CH	6.34, br d (1.76)		C-2, 3, 4a, 9a	
4a	157.3, C				
5, 5'	130.8, C				
6	149.6, C				
7	132.1, C				
8	142.6, C				
8a	108.5, C				
9	181.3, C				
9a	102.6, C				
10a	146.6, C				
1'	163.5, C				
2'	98.2, CH	6.13, d (1.91)		C-1', 3', 4', 9a'	
3'	165.3, C				
4'	93.5, CH	6.35, d (1.91)		C-2', 3', 4a', 9a'	
4a'	156.7, C				
6'	151.1, C				
7'	113.4, CH	6.60, s		C-8, 11, 5', 6', 9', 8a', 10a'	H-12
8'	137.3, C				
8a'	112.0, C				
9'	183.3, C				
9a'	102.5, C				
10a'	147.0, C				

Table S3. continued

Position	δ_C , type	δ_H , mult (J_{Hz})	COSY	HMBC	NOESY
11	41.8, CH	6.45, d (9.83)	H-12	C-6, 7, 8, 12, 13, 6', 7', 8', 8a'	H _{ax} -14, H-19
12	61.1, CH	2.47, m	H-11, 17	C-8, 11, 13, 14, 16, 17, 18	H-17, 18, 7'
13	33.0, C				
14	40.3, H _{ax} -CH ₂	2.40, br d (17.4)			H-11, 19
14	40.3, H _{eq} -CH ₂	1.53, br d (17.4)		C-12, 13, 15, 16, 18, 20	H-18, 19
15	131.3, C				
16	122.4, CH	5.34, m	H-17	C-12, 14, 20	H-20
17	45.0, CH	4.68, m	H-12, 16	C-6, 8	H-12, 18
18	29.1, CH ₃	0.97, s		C-11, 12, 13, 14	H-12, 17, 19, H _{eq} -14
19	29.1, CH ₃	0.65, s		C-12, 13, 14, 15, 18	H-11, 18, H _{eq} -14, H _{ax} -14
20	24.3, CH ₃	1.60, s		C-14, 15, 16	H-16
OH-1	OH	13.63, s		C-1, 2, 9a	
OH-1'	OH	13.40, s		C-1', 2', 9a'	

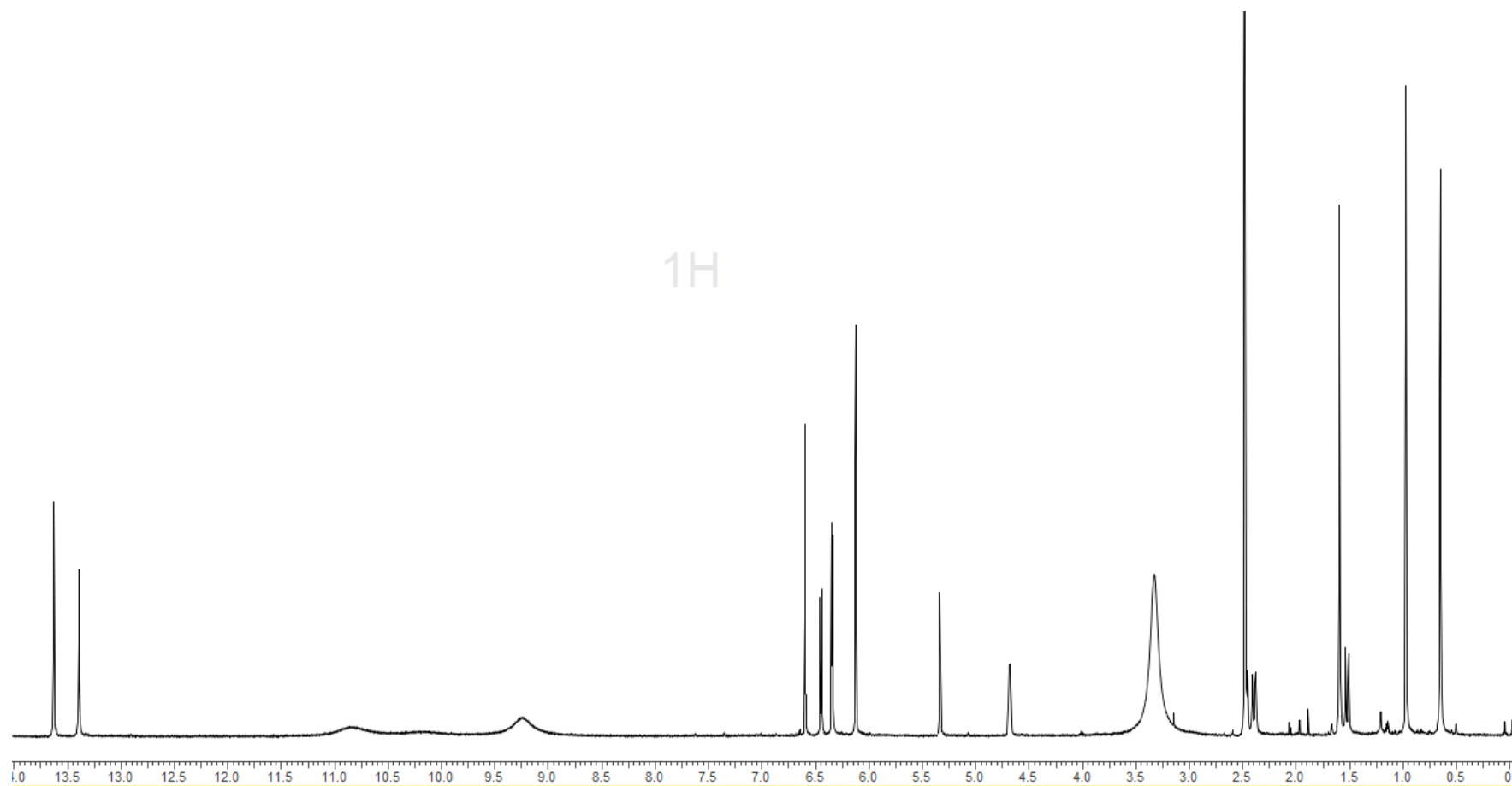


Figure S1. ^1H NMR spectrum of compound **1**

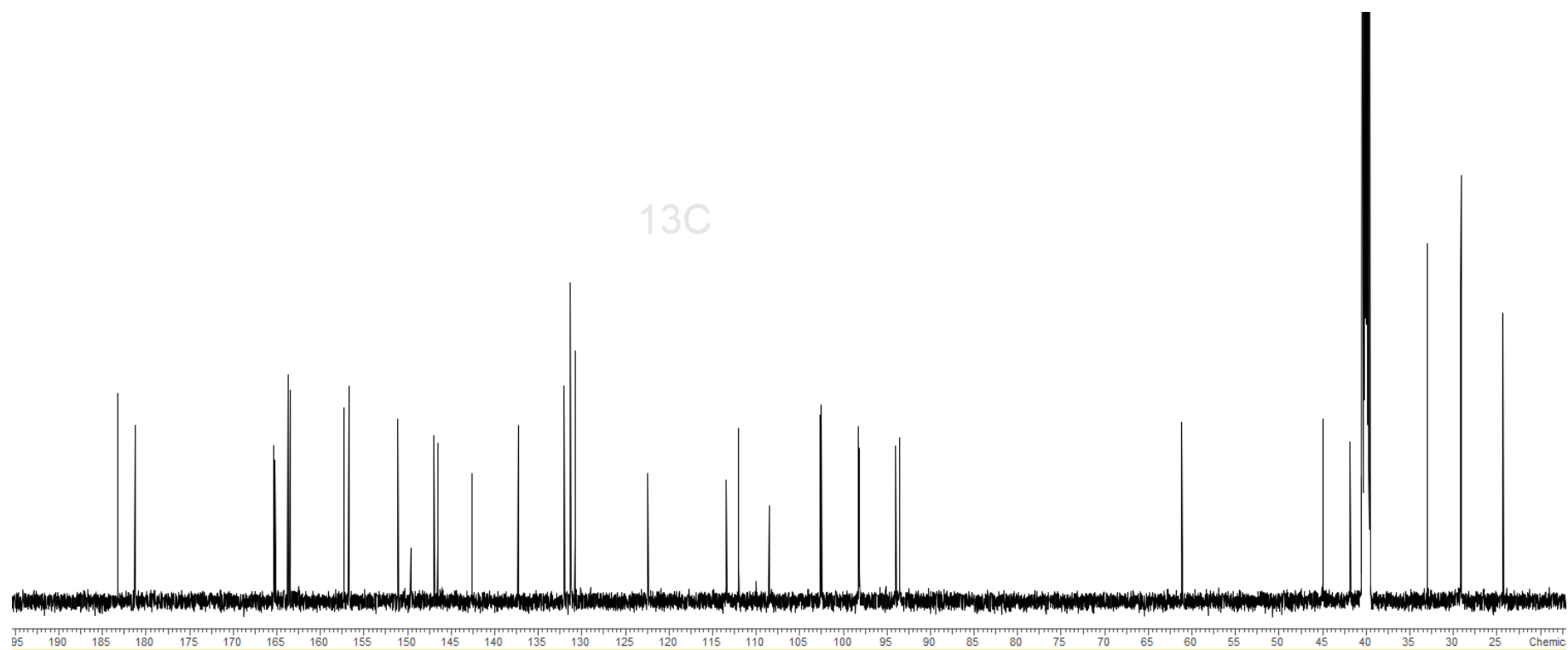


Figure S2. ¹³C NMR spectrum of compound **1**

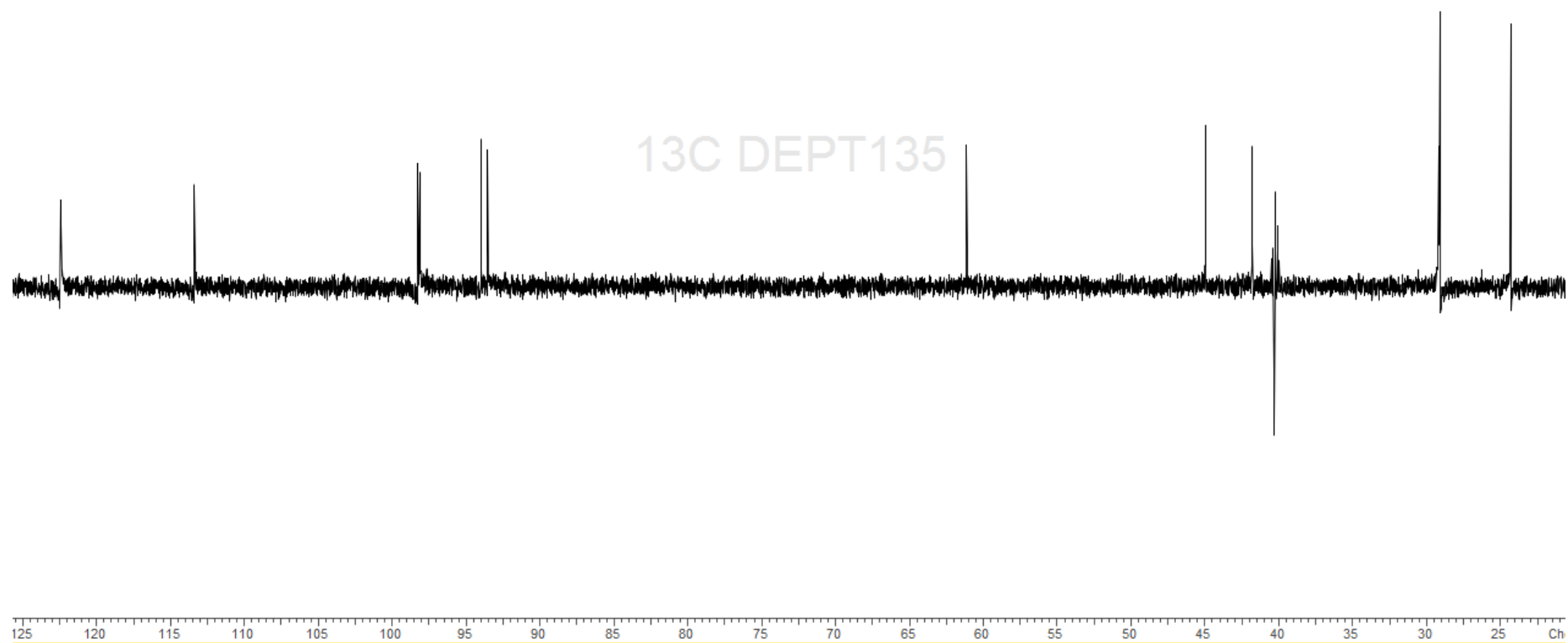


Figure S3. DEPT135 spectrum of compound **1**

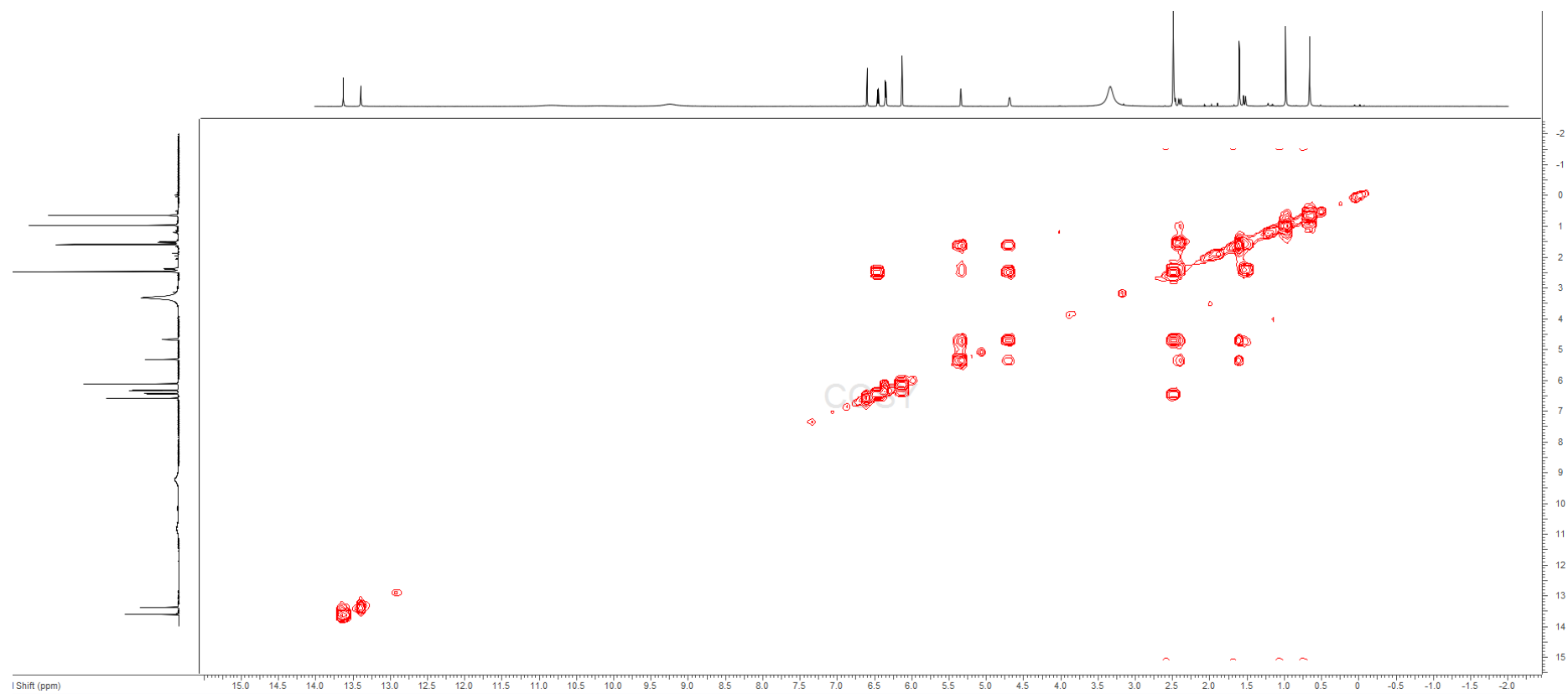


Figure S4. COSY spectrum of compound **1**

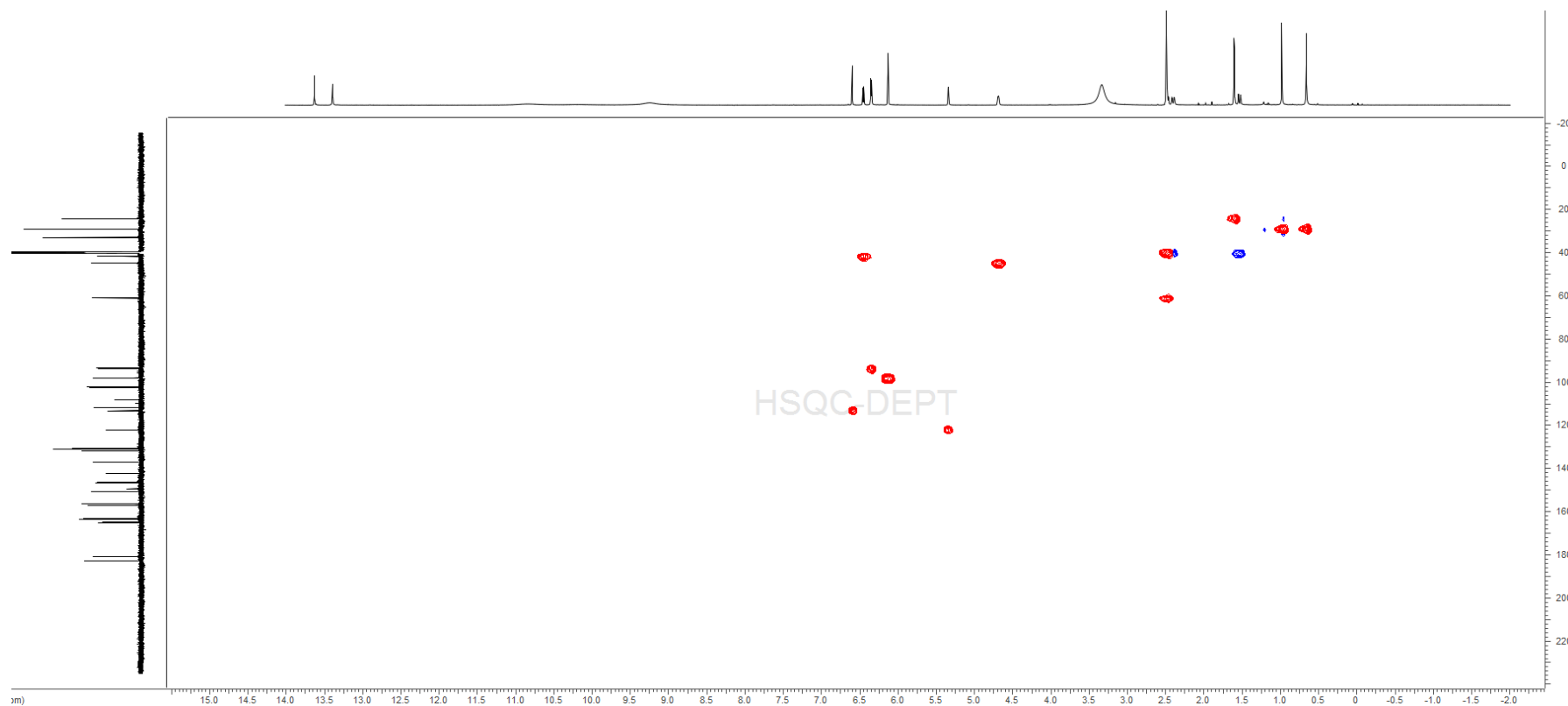


Figure S5. HSQC spectrum of compound **1**

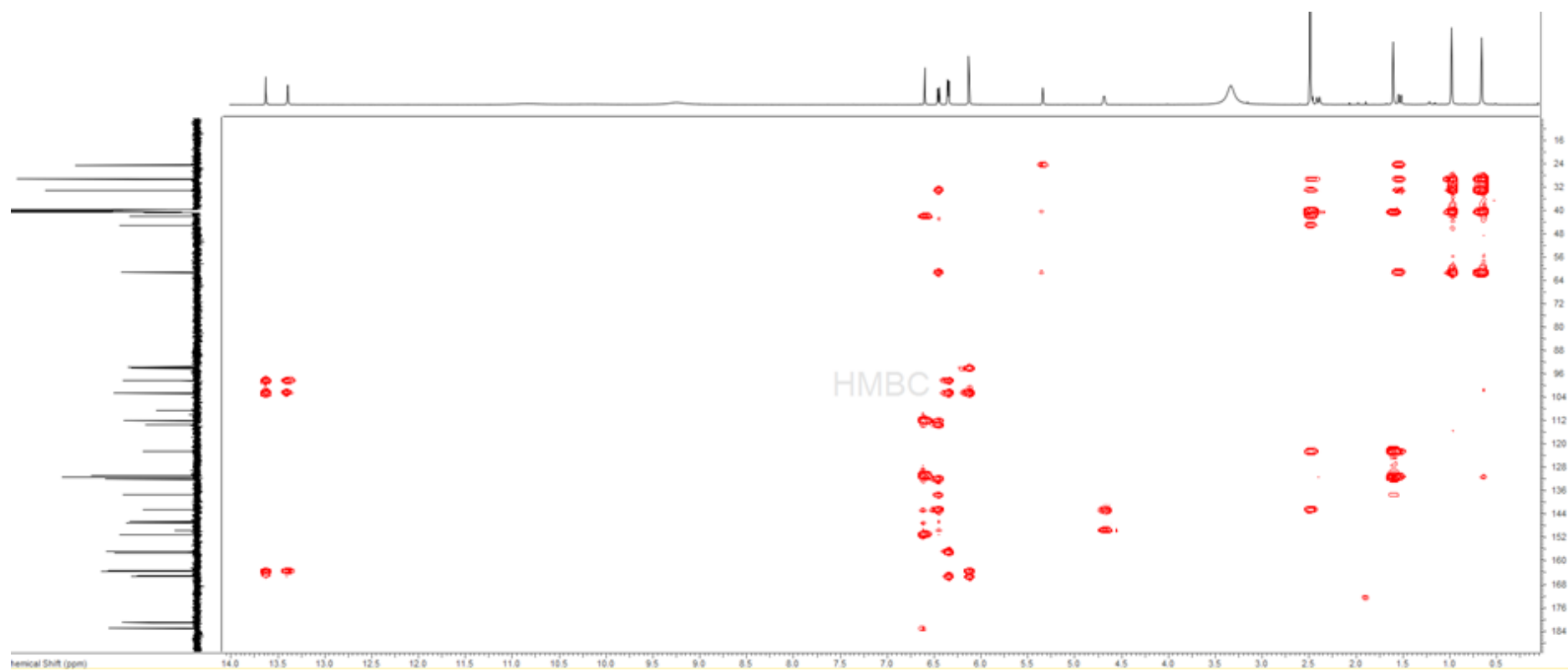


Figure S6. HMBC spectrum of compound 1

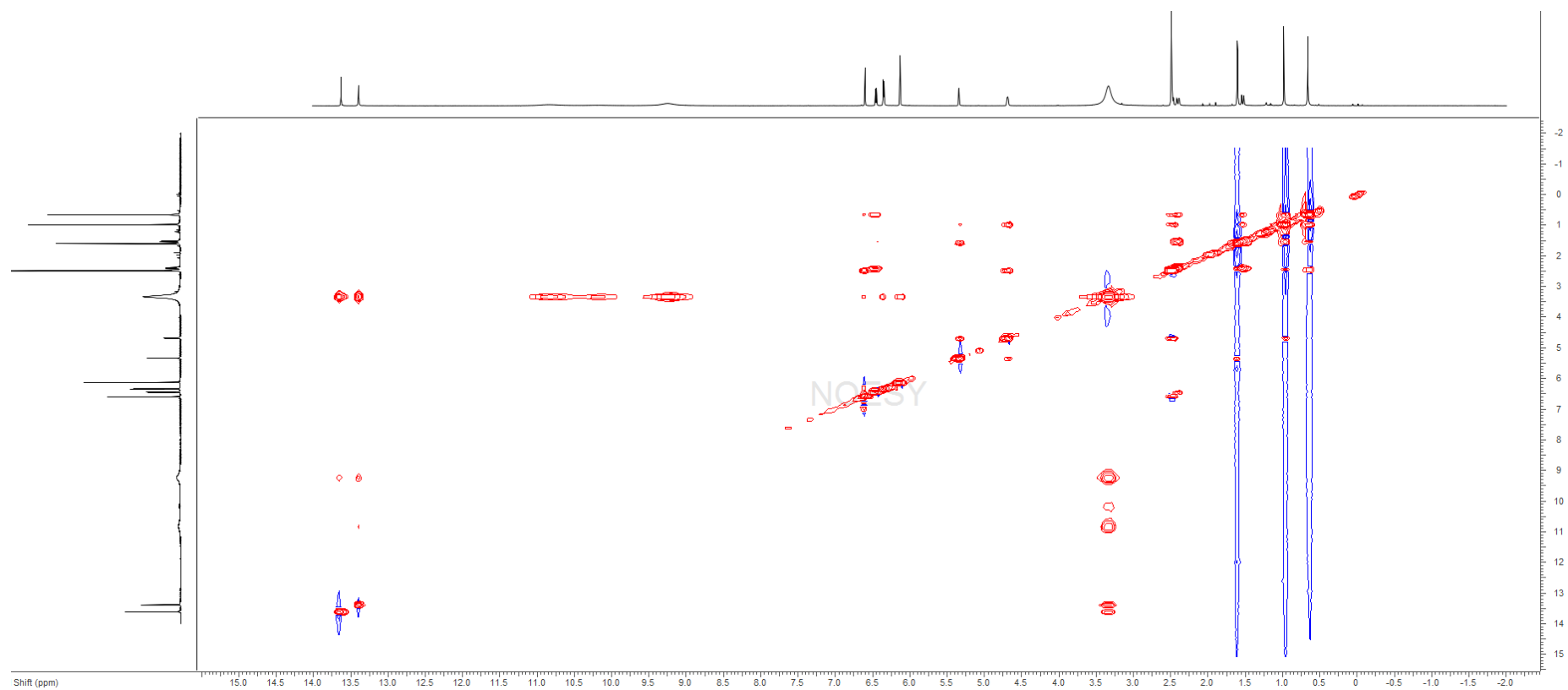
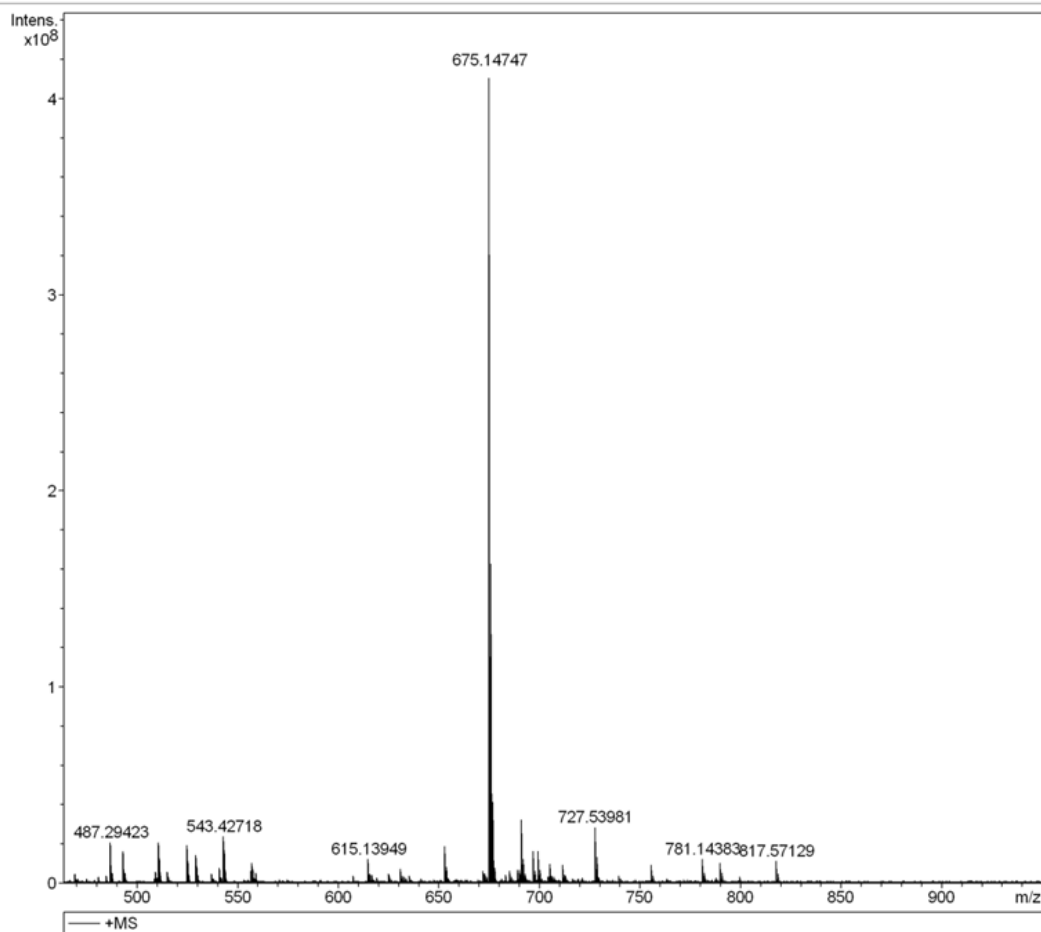


Figure S7. NOESY spectrum of compound **1**

Acquisition Parameter

Polarity	Positive	Source	ESI	No. of Laser Shots	20
Averaged Scans	8	No. of Cell Fills	1	Laser Power	51.0 %
Broadband Low Mass	100.4 m/z	End Plate	3900.0 V	MALDI Plate	300.0 V
Broadband High Mass	3000.0 m/z	Capillary Entrance	4400.0 V	Imaging Spot Diameter	2000.0 μ m
Acquisition Mode	Single MS	Skimmer 1	36.0 V		
Pulse Program	basic	Drying Gas Temperature	200.0 $^{\circ}$ C	Calibration Date	Sat Jul 29 06:30:12 2017
Source Accumulation	0.0 sec	Drying Gas Flow Rate	4.0 L/min	Data Acquisition Size	1048576
Ion Accumulation Time	1.0 sec	Nebulizer Gas Flow Rate	1.0 L/min	Apodization	Sine-Bell Multiplication
Flight Time to Acq. Cell	0.0 sec				

Figure S8. HRESIMS spectrum of compound **1**

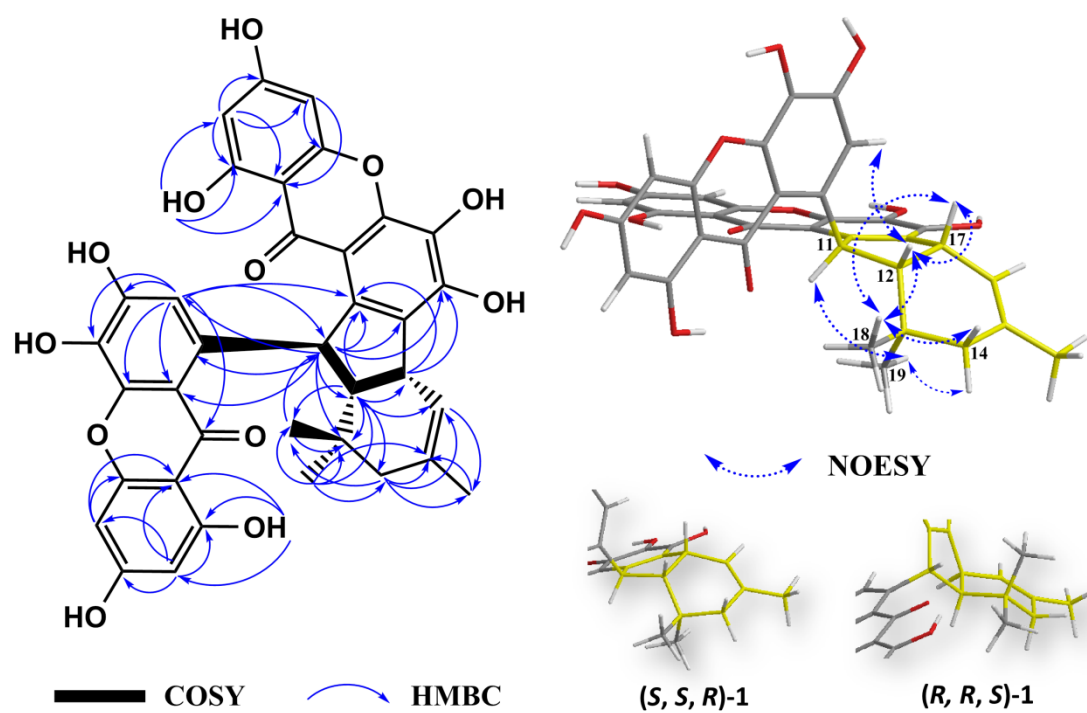


Figure S9. Key COSY, HMBC and NOESY correlations of **1** and configuration of two possible isomers of **1**

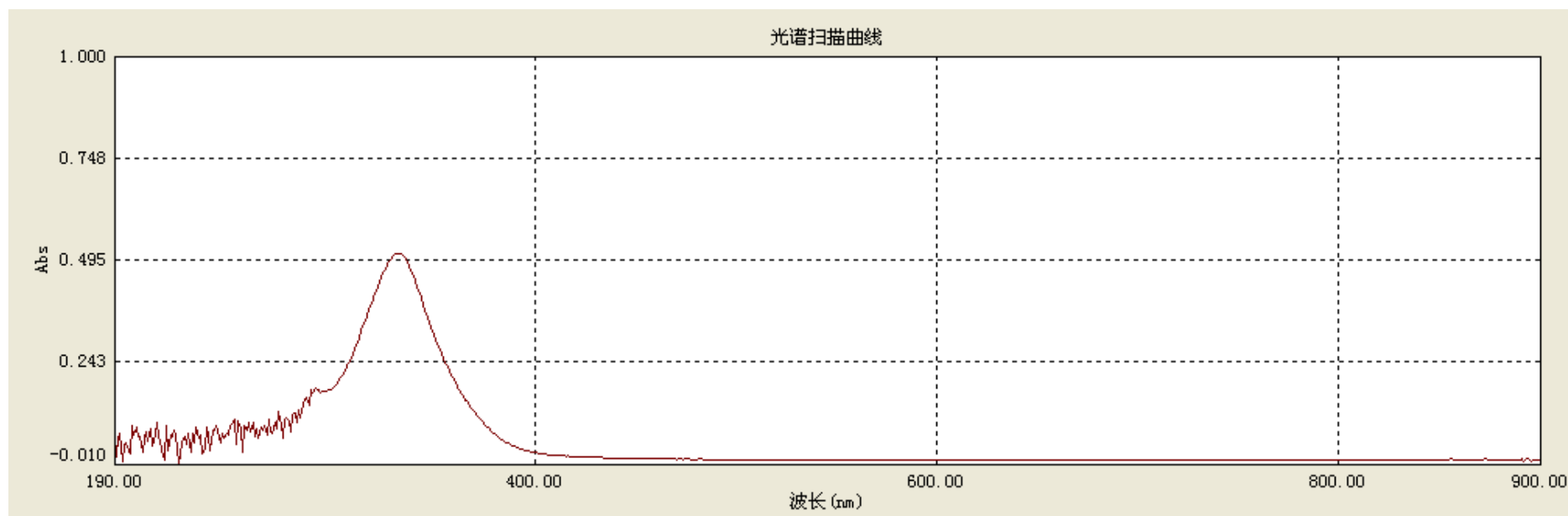


Figure S10. UV spectrum of compound **1**

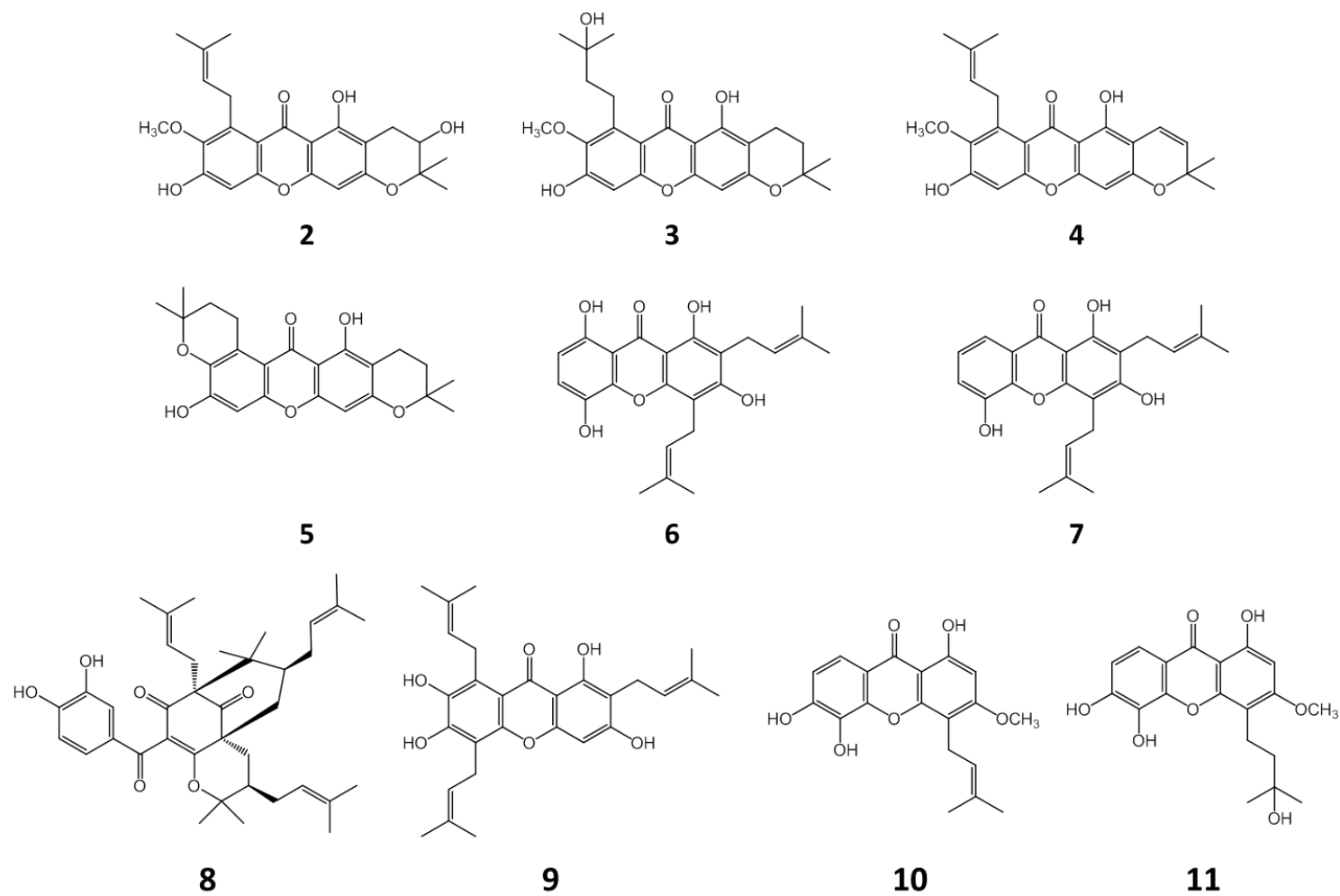


Figure S11. Chemical structures of compounds 2-11

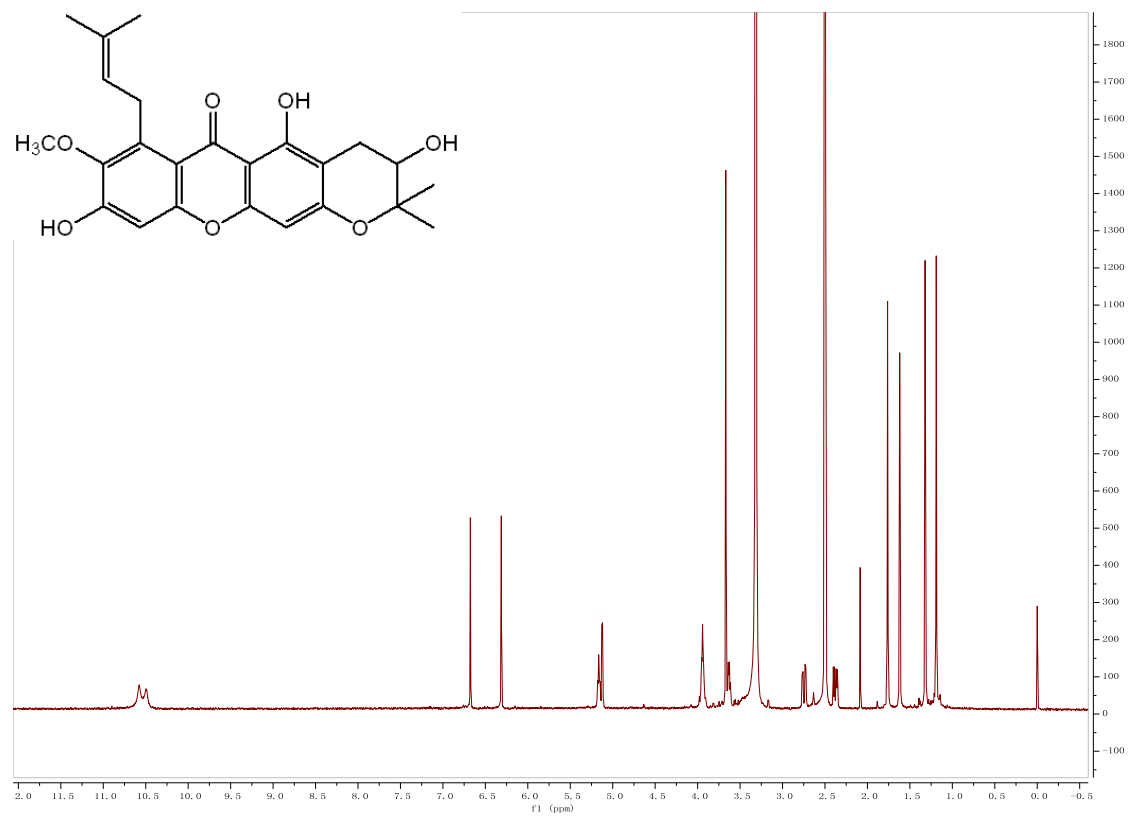


Figure S12. ^1H NMR spectrum of compound 2

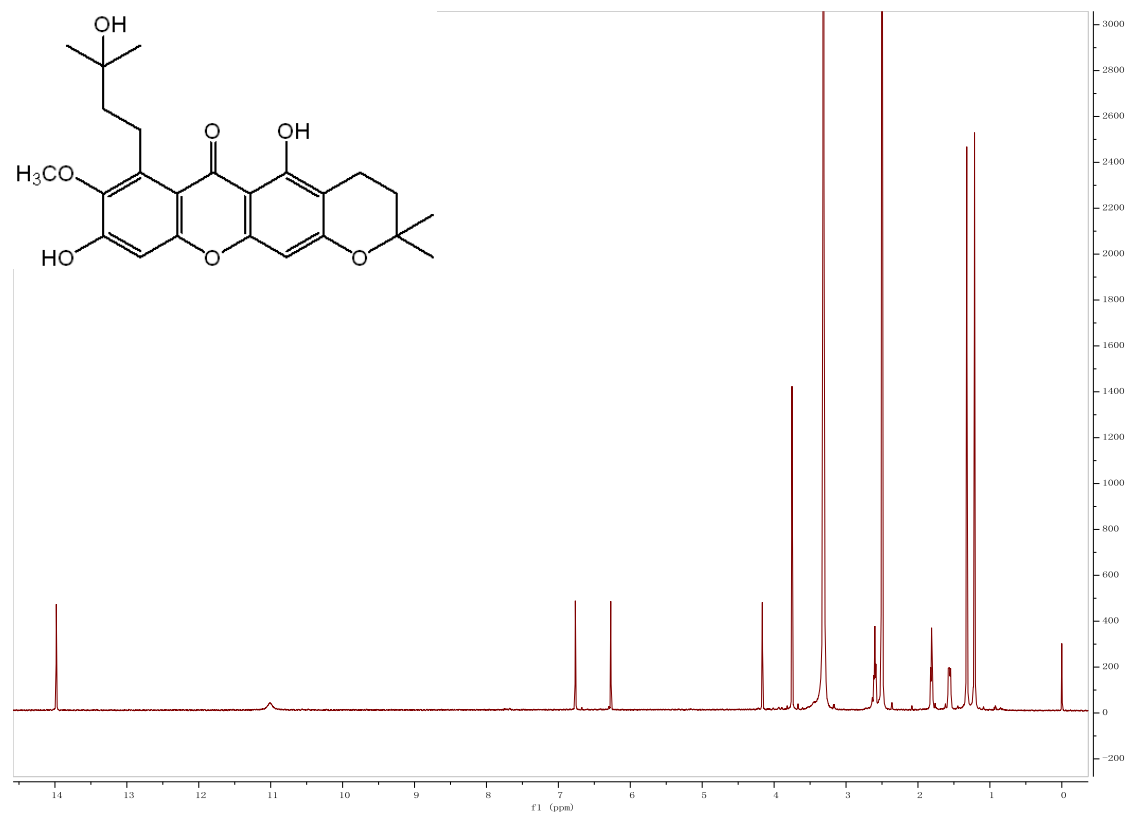


Figure **S13**. ^1H NMR spectrum of compound **3**

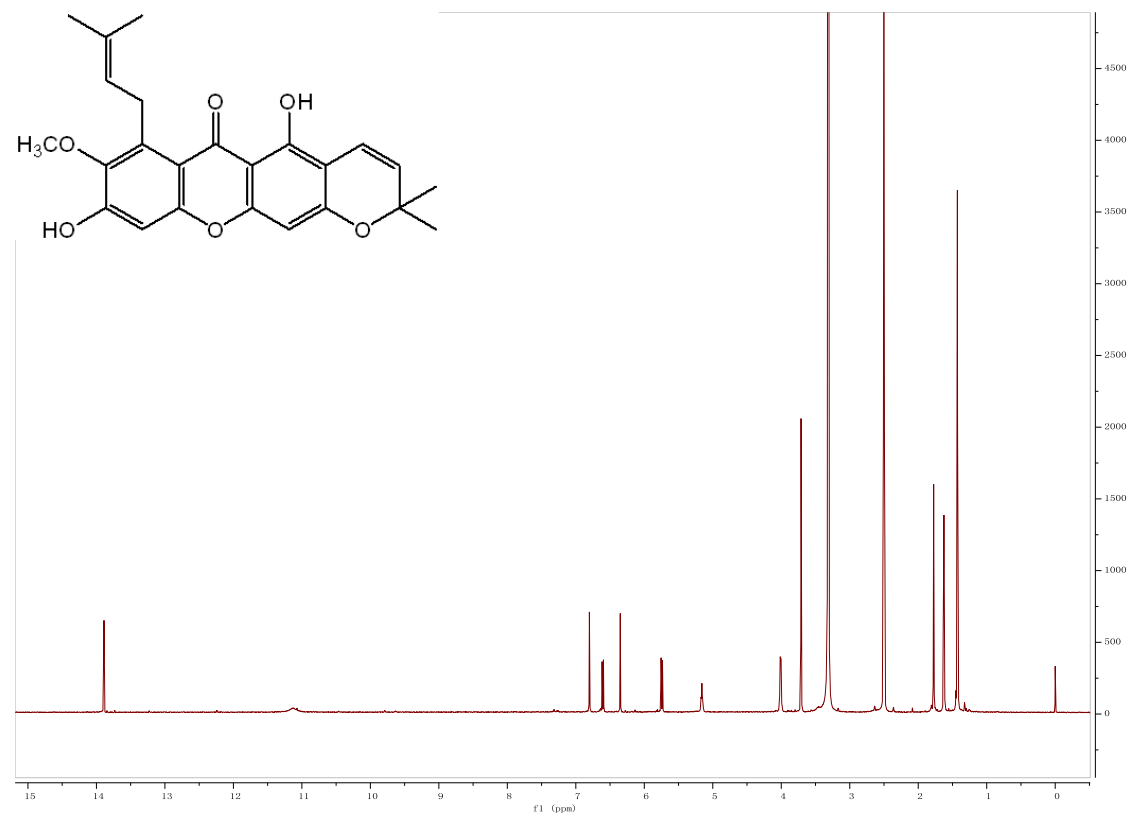


Figure S14. ¹H NMR spectrum of compound **4**

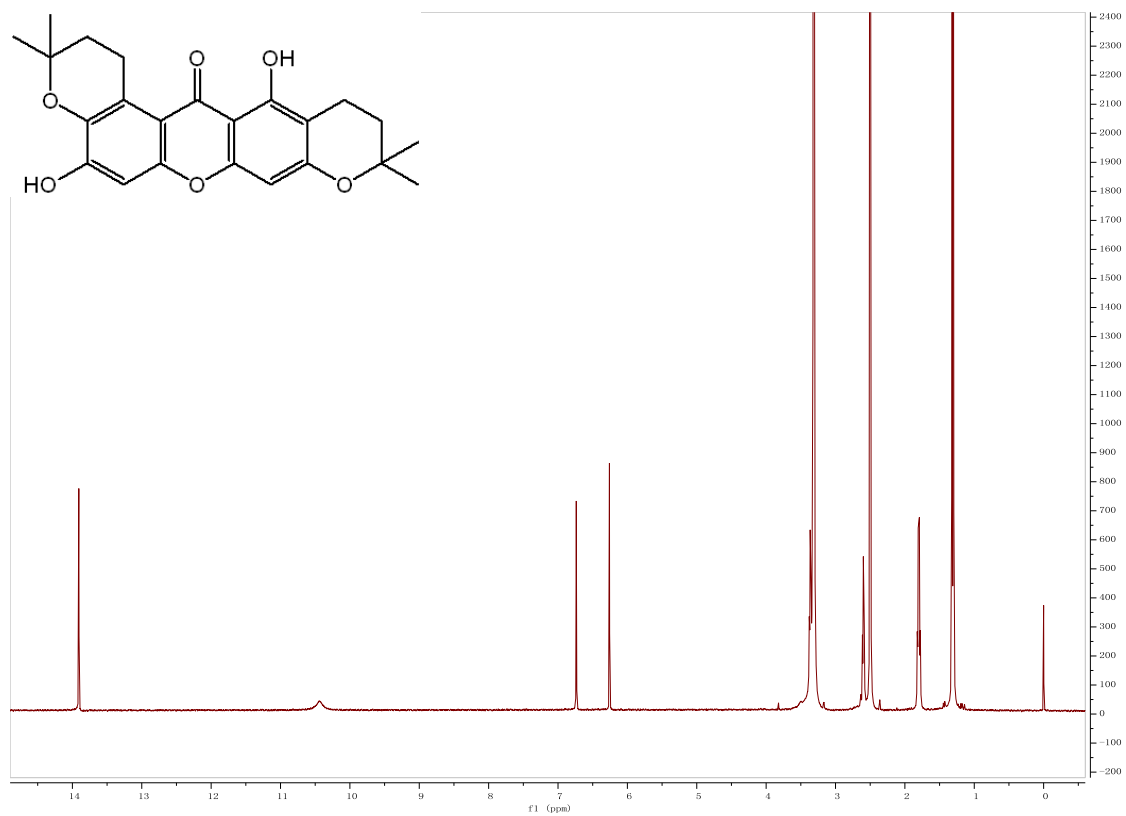


Figure S15. ¹H NMR spectrum of compound 5

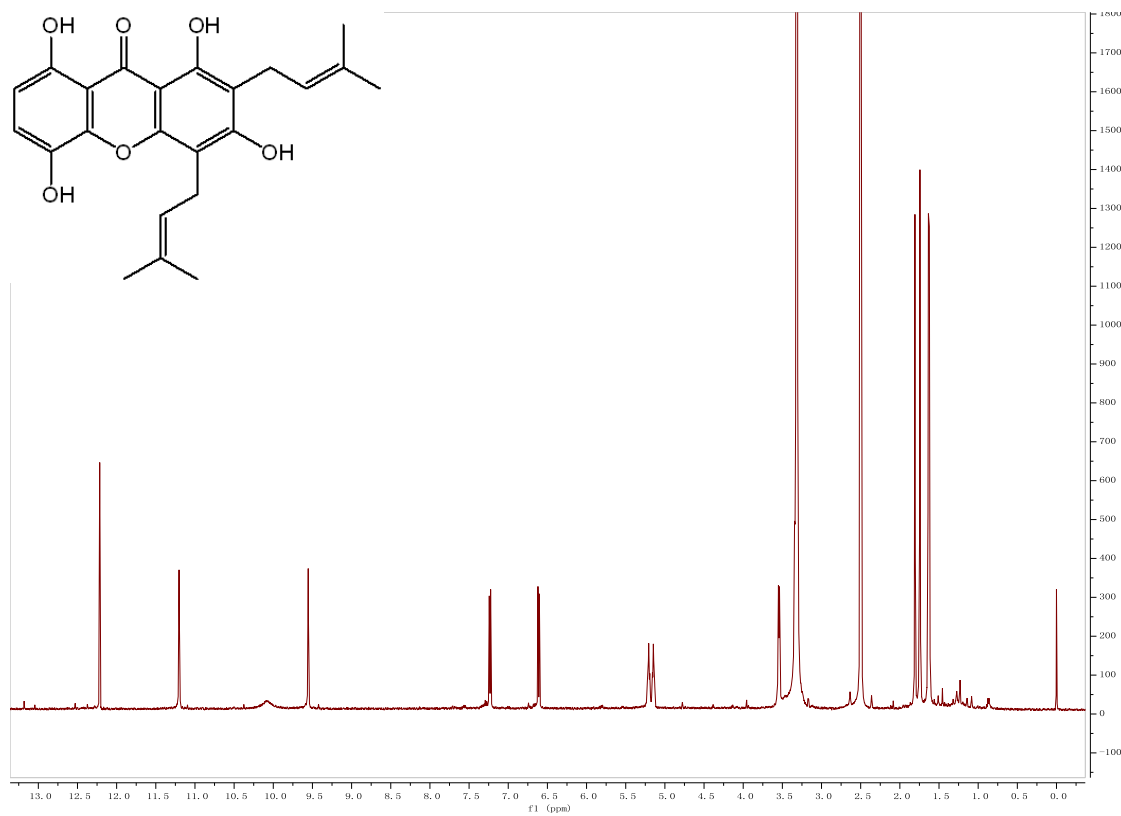


Figure S16. ^1H NMR spectrum of compound 6

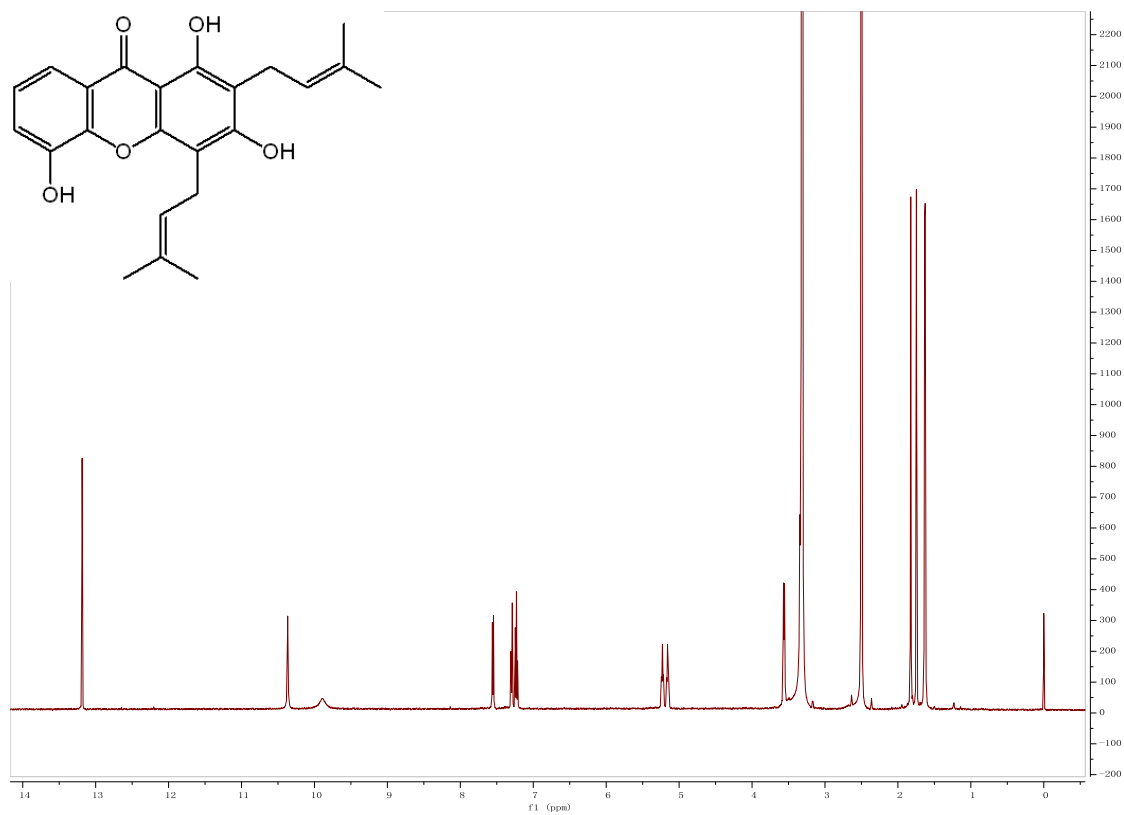


Figure S17. ¹H NMR spectrum of compound 7

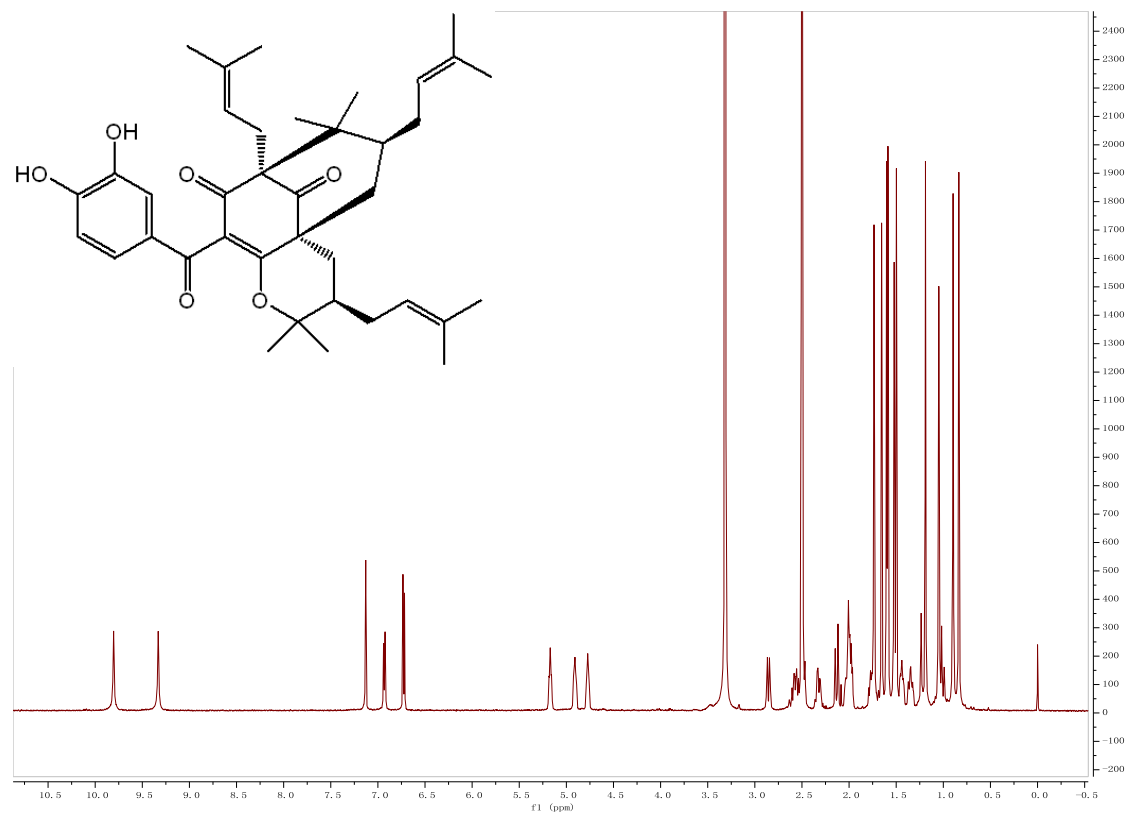


Figure S18. ^1H NMR spectrum of compound 8

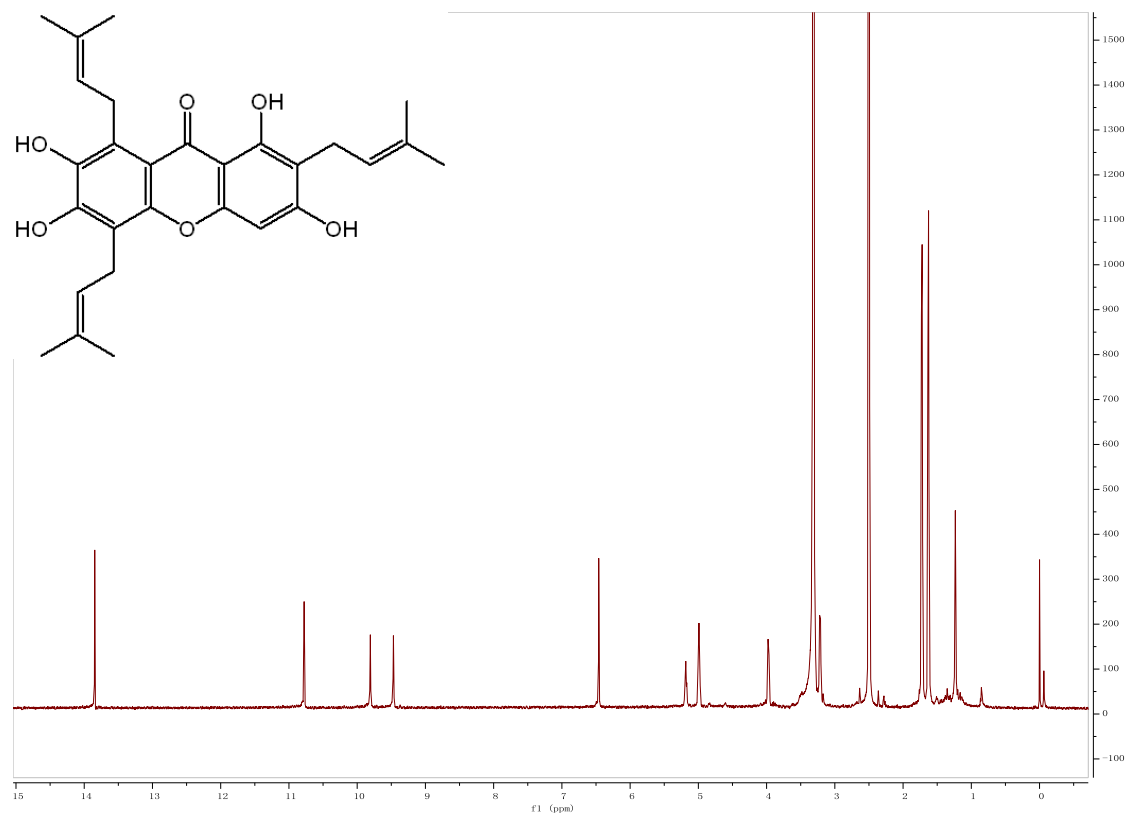


Figure S19. ^1H NMR spectrum of compound **9**

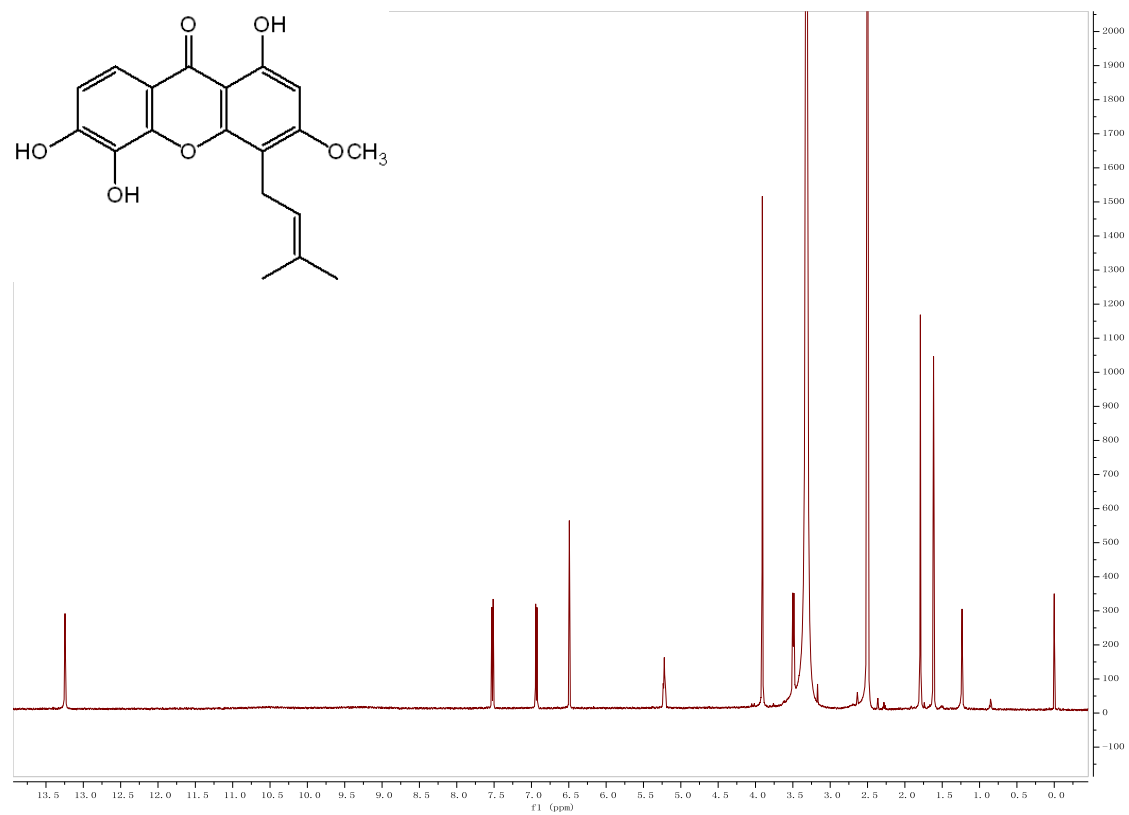


Figure S20. ^1H NMR spectrum of compound **10**

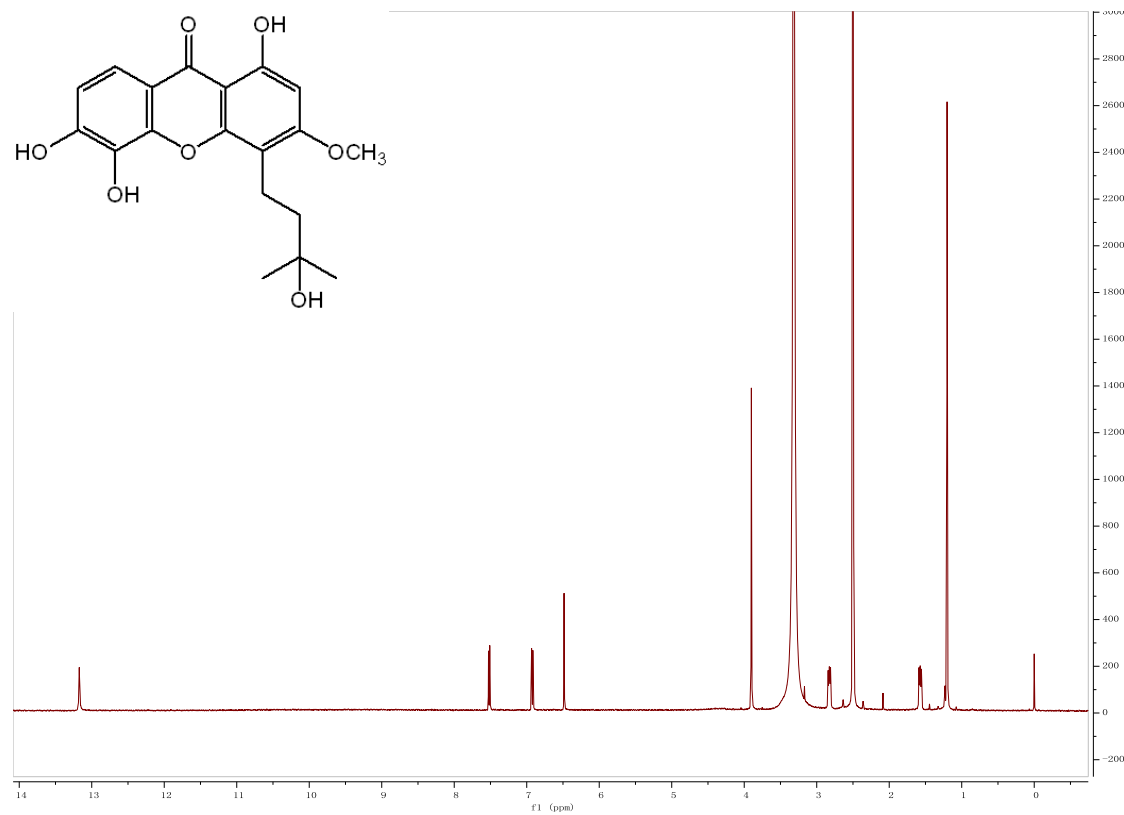


Figure S21. ^1H NMR spectrum of compound **11**

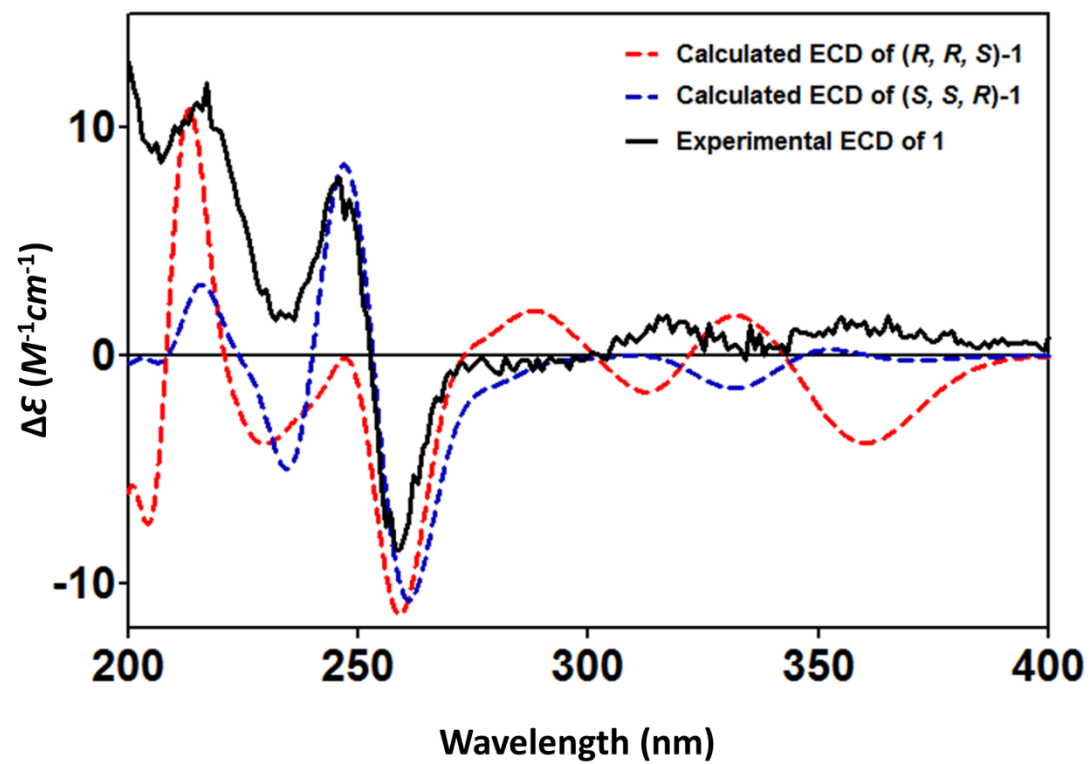


Figure S22. Calculated and Experimental ECD of **1**